PERGAMON

International Journal of Plasticity 17 (2001) 65–85

INTERNATIONAL JOURNAL OF Plasticity

www.elsevier.com/locate/ijplas

Polycrystal modelling of IF-Ti steel under complex loading path

T. Hoc [a,*], S. Forest [b]

[a] *Laboratoire de Mécanique des Sols, Structures et Matériaux, Ecole Centrale Paris, UMR 8579, Grande Voie des Vignes, 92295 Châtenay-Malabry cedex, France*

[b] *Centre des Matériaux, UMR 7633, Ecole des Mines Paris, BP 87, 91003 EVRY, cedex, France*

Received in final revised form 15 February 2000

Abstract

Simple and complex loadings were performed on a IF-Ti steel in order to test different hardening laws. The different loading paths included uniaxial tension, plane strain, cyclic shear plane and plane strain tests followed by uniaxial tensile tests. Our aim was to determine the hardening law from these tests. For this purpose a polycrystalline self-consistent model was introduced. In this model an explicit concentration law and an intragranular behaviour based on the evolutions of physical parameters were proposed. Local objective frames were introduced to extend constitutive equations developed at small strains, to the finite strain framework. The identification of the physical parameters was performed thanks to an inverse method and led to values in good agreement with literature. For the different tests, macroscopic stresses and texture evolutions were computed and compared to experimental results. Initial and prestrain yield stresses surfaces were calculated. These different simulations pointed out for complex loading paths the necessity of an accurate description of the microplasticity mechanisms,in terms of slip systems, hardening matrix and evolution of dislocations densities on each slip system.

Keywords: B. Polycrystalline material; IF-Ti steel; Cyclic shear plane

1. Introduction

In recent years, particular attention has been paid to the anisotropic work-hardening of polycrystalline metals submitted to changes of loading path at large strains. Most of the previous studies were devoted to the modelling of a cold forming process and to the understanding of the underlying physical mechanisms (e.g. microstructure evolution

* Corresponding author. Tel.: +33-1-41131616.

E-mail address: hoc@mssmat.ecp.fr (T. Hoc).

0749-6419/01/$ - see front matter
PII: S0749-6419(00)00019-X

and texture evolution). In order to investigate the evolution of the anisotropic behavior of materials during complex loading modes, involved in cold forming operation, combinations of sequences of more simple loadings paths such as tension, plane tension, rolling and simple shear were often considered (Ghosh and Backofen, 1973; Korbel and Martin, 1988; Rauch and G'sell, 1989). Such investigations were performed to differentiate the effects of microstructural hardening and textural hardening. On one hand, many authors assumed that plastic behavior of material mainly depends on the microstructural evolution, the texture evolution during pre-strain being negligible. For most of the proposed models, the microstructural evolution, was reduced to a single parameter (total dislocation density). This description commonly accepted for monotonous deformation, was not sufficient to describe the transient stage associated with the reorganisation of dislocation microstructures. According to experimental evidence, different models, taking into account polarity of persistent dislocation structures at a macroscopic scale (Hiwatashi et al., 1998; Hu et al., 1992) or microscopic scale (Rauch and Thuillier, 1993), were elaborated in order to predict a softening after a change of loading path.

On the other hand, the modelling of the mechanical behavior of metal polycrystals with a micromechanical approach received a particular attention in the last 10 years (Berveiller and Zaoui, 1998). The main difficulty raised from this type of approach is the choice of the pertinent scale and of the critical mechanisms. In the specific case of metallic polycrystalline models, the description of the hardening law or (and) of the texture were generally simplified in order to reduce the time of computations.

The aim of the present paper is to test different hardening laws, in order to determine their ability to describe homogeneous macroscopic behavior of the material under various monotonous and sequential loading conditions. A micro-mechanical approach is proposed in Section 2, based on the description of the single crystal kinematics, and an explicit concentration law is adopted, allowing the overcoming of the difficulties of self-consistent modelling in elastoviscoplasticity under complex loading path. Moreover, an intragranular behavior depending on the evolutions of physical parameters like dislocation densities on each slip system is introduced. Section 3 is devoted to the modelling of microstructure and texture evolutions during monotonic deformation and strain path changes. It will be emphasized that particular attention should be paid to the value of physical parameters such as latent hardening, dislocation density.

2. Plasticity of BCC metals

2.1. Polycrystalline approach at small strains

In the following, Y, $\overrightarrow{Y}$, $\underline{Y}$ and $\underline{\underline{Y}}$ correspond to a scalar, a vector, a second-rank and a four-rank tensor, respectively.

2.1.1. Self-consistent scheme

The self-consistent approach is an efficient tool to derive the global mechanical behavior of aggregates from the mechanical behavior of the phases. In the case of

metal polycrystals, the phases (g) are built up with families of grains. The orientation of which lies between (g) and (g + dg) and the volume fraction is (f_g). In this approach, each family of grains is considered as an inclusion embedded in an infinite matrix (homogeneous equivalent medium) submitted to homogeneous boundary conditions. The self-consistent scheme allows the determination of the average homogeneous stress and the strain fields $\underset{\sim}{\sigma}^g$ and $\underset{\sim}{\varepsilon}^g$ in each phases (g), these fields representing the average interaction between the phase (grain) and the homogeneous equivalent medium. This self-consistent approach does not take into account the position of each grain in the aggregate, the exact shape, the local effect of grain boundaries and of the grain size.

In the case of isotropic elasticity, we have:

$$\underset{\sim}{E}^p = \sum_{g\in G} f_g \underset{\sim}{\varepsilon}^{gp}; \quad \underset{\sim}{\Sigma} = \sum_{g\in G} f_g \underset{\sim}{\sigma}^g = 2\mu \left\{ \underset{\approx}{I} + \frac{\nu}{1-2\nu} \underset{\sim}{1} \otimes \underset{\sim}{1} \right\} \left(\underset{\sim}{E} - \underset{\sim}{E}^p \right) \tag{1}$$

where μ is Coulomb's modulus and ν the Poisson ratio. The macroscopic plastic strain $\underset{\sim}{E}^p$ is the average of the local plastic strain $\underset{\sim}{\varepsilon}^{gp}$ of all grains g and the macroscopic stress $\underset{\sim}{\Sigma}$ can be deduced from Hooke's law. It is worth noting that this formulation is developed at small strains.

A rigorous treatment of this problem was proposed by Hill (1965), for time independent plasticity but led to a complex implicit integral differential equation. In the case of isotropic elastoplasticity and radial monotonous loading, Berveiller and Zaoui (1979) developed for a spherical inclusion, an explicit concentration rule given by:

$$\underset{\sim}{\sigma}^g = \underset{\sim}{\Sigma} + 2\mu(1-\beta)\alpha\left(\underset{\sim}{E}^p - \underset{\sim}{\varepsilon}^{pg} \right) \text{with} \frac{1}{\alpha} \simeq 1 + \frac{3}{2}\mu \frac{\left\| \underset{\sim}{E}^p \right\|}{J_2\left(\underset{\sim}{\Sigma} \right)} \tag{2}$$

In this formulation, β is close to $\frac{1}{2}$, $\left\| \underset{\sim}{\bullet} \right\| = \sqrt{\frac{2}{3} \underset{\sim}{\bullet} : \underset{\sim}{\bullet}}$ and α is the plastic accommodation factor. This factor, close to 1, at the beginning of the deformation, allows to reduce intergranular stresses for further deformation. This formulation is similar to Kröner's formulation (Kroner, 1961) with $\alpha = 1$.

The concentration rule proposed by Berveiller and Zaoui is suitable for monotonous loading but does not allow the forecasting of mechanical behavior after changes of loading path in anisotropic polycrystals. In this work, we choose the concentration rule proposed by P. Pilvin (1994) suitable for complex cyclic loading simulations within the framework elastoviscoplasticity.

This concentration rule is a priori given under an explicit form by:

$$\underset{\sim}{\sigma}^g = \underset{\sim}{\Sigma} + \mu\left(\underset{\sim}{B} - \underset{\sim}{\beta}^g \right) \text{ with } \underset{\sim}{B} = \sum_{g\in G} f_g \underset{\sim}{\beta}^g \tag{3}$$

In this formulation, $\underset{\sim}{\beta}^g$ is a local non linear kinematic variable bound to phase (g), which describes interaction between grains and matrix. Its effect is to reduce internal

stresses and to give a suitable description of cyclic test in elastoviscoplastic framework. $\underset{\sim}{\beta}^g$ evolution is given by:

$$\dot{\underset{\sim}{\beta}}^g = \dot{\underset{\sim}{\varepsilon}}^{pg} - D\left(\underset{\sim}{\beta}^g - \delta\underset{\sim}{\varepsilon}^{pg}\right)\left\|\dot{\underset{\sim}{\varepsilon}}^{pg}\right\| \tag{4}$$

where D and δ are two tuning parameters whose validity will be discussed in Section 3.4.

2.1.2. Viscoplastic flow rule

The condition of activation of a slip system (s) of phase (g) is given by Schmid's law:

$$|\tau^{sg}| \geqslant \tau_c^{sg} \tag{5}$$

where τ_c^{sg} is the critical shear stress, which depends on the structural variables and temperature, while τ^{sg} is the resolved shear stress on slip system (s) given by:

$$\tau^{sg} = \underset{\sim}{\sigma}^g : (\vec{m}^{sg} \otimes \vec{n}^{sg}) \tag{6}$$

where $\vec{m}^{sg}$ and $\vec{n}^{sg}$ are respectively the slip direction and normal of system (s). The flow rule is related to the thermal dependence of the dislocation motion which is described by the theory of thermally activated dislocation glide (Teodosiu and Sidoroff, 1976). However, the relation between the applied resolved shear stress τ^{sg} and the shear strain rate $\dot{\gamma}^{sg}$ can be approximated, for viscoplastic glide, by the power law (Cailletaud, 1991):

$$\begin{aligned} &\dot{\gamma}^{sg} = \dot{\gamma}_o\left(\frac{|\tau^{sg}| - \tau_c^{sg}}{\tau_0}\right)^n \operatorname{sgn}(\tau^{sg}) \quad \text{if} \quad |\tau^{sg}| > \tau_c^{sg} \\ &\dot{\gamma}^{sg} = 0 \quad \text{otherwise} \end{aligned} \tag{7}$$

where $\dot{\gamma}_o$ is a reference strain rate, exponent n is close to 10 at room temperature for metallic materials and τ_o is the friction stress which depends on temperature.

2.1.3. Hardening laws

Hardening characteristics of the material depend on the microplasticity mechanisms such as the interactions between the different slip systems (activated and latent slip systems).

Hardening is ruled by the stacking fault energy of the metal, the density of dislocations, the mean free path of the activated dislocations. In a given grain, the hardening and its critical resolved stress evolution with increasing deformation is generally introduced into the expression of the critical shear stress by:

$$\dot{\tau}_c^{sg} = \sum_u h^{su}\left|\dot{\gamma}^{ug}\right| \tag{8}$$

where the component $h^{(su)}$ of the hardening matrix corresponds to the nature of interactions between the density of dislocations (s) and the dislocation (u) which have produced a crystallographical shear amplitude rate $|\dot{\gamma}^{ug}|$. The identification of the hardening matrix, assumed homogeneous in a grain, is essential in the case of sequential tests, where latent slip systems during the first loading become activated slip systems during the second path.

The form of the hardening matrix chosen in this paper is similar to the one suggested by Franciosi (1984, 1985) for B.C.C. single crystals and small strains. In this model, the terms h^{su} increase with the strain amplitude and present a sharp variation at the beginning of the deformation, then tends to a constant. A monotonic dependence on internal variables, such as average density of dislocations is assumed. Our aim is to determine the intragranular hardening matrix of the polycrystal from different experimental stress–strain curves obtained during monotonous and sequential loadings. In the following identification, the hardening matrix corresponds to the case of a single crystal embedded in a matrix and is deduced from different physicals laws given below. The evolution of the total dislocation density, based on Orowan's relation and annihilation process of dislocation dipoles (Essman and Hughrabi, 1979), is given by the evolution law:

$$\dot{\rho}^{sg} = \frac{1}{b}\left(\frac{1}{L^{sg}} - G_c \rho^{sg}\right)|\dot{\gamma}^{sg}| \tag{9}$$

where b is the magnitude of the Burgers vector, G_c a parameter proportional to the characteristic length associated with the annihilation process of dislocation dipoles, and L^{sg} the mean free path of system (s) which can be expressed by:

$$L^{sg} = K\left(\sum_{u \neq s} \rho^{gu}\right)^{-\frac{1}{2}} \tag{10}$$

where ρ^u is total dislocation density on latent systems (u). In this formulation, K is a material parameter and only the dislocation–dislocation interactions (forest interaction) are taken into account.

The critical shear stress on system (s) can be related to the dislocation densities evolution by the relation:

$$\tau_c^{sg} = \tau_o + \mu b\left(\sum_u a^{su}\rho^u\right)^{\frac{1}{2}} \tag{11}$$

where a^{su} characterizes the interactions between two densities of dislocations (s) and (u) and is constant.

By differentiation of Eq. (11) with respect to time, the phenomenological law (8) is obtained and the hardening matrix is now given by:

$$h^{su} = \frac{\mu}{2} a^{su} \left(\sum_l a^{sl} \rho^l \right)^{-\frac{1}{2}} \left\{ \frac{1}{K} \left(\sum_{l \neq u} \rho^l \right)^{\frac{1}{2}} - G_c \rho^u \right\} \tag{12}$$

The hardening matrix explicitly depends on the current values of the dislocation densities and in this work, such formulation characterizes the interaction dislocation–dislocation.

2.2. Kinematics of polycrystal at finite deformations

The previous constitutive framework for polycrystalline plasticity must be extended to large deformations. For this purpose, we have chosen to use the so-called local objective space frames (Ladeveze, 1980). An example of such a local objective space frame is the corotational frame associated with the skew-symmetric part of velocity gradient $\underset{\sim}{L}$. This method can also be applied to polycrystals (Forest, 1996). As a matter of fact, a local objective frame like the corotational one enables us to get rid of rotations that do not intervene in the material response. Such a frame does not contain any physical information, so that an additional treatment of lattice rotations is necessary.

The description of polycrystal plasticity using the corotational frame proposed by Forest (1996) is based on a scheme presenting two levels, a macroscopic one, corresponding to the polycrystal and a more microscopic one corresponding to the grains.

Let C^0, C and C^c be respectively the initial space frame, the current space frame and the corotational space frame, defined at the macroscopic level. For polycrystals, the microscopic level is composed of n lattice space frames $c_1^{\#}, c_2^{\#}, \cdots, c_n^{\#}$, corresponding to the n phases (grains). According to Forest and Pilvin (1999), the hereabove scheme gives, for single crystal and small elastic strains, the same numerical result as the classical decomposition of deformation in Mandel's theory (1982). The configurations C^c and C, $c_i^{\#}$ and C^c (see Fig. 1) are related by rotations Q^c and $Q_i^{\#}$ respectively.

The corotational frame is defined by ${}^c\dot{\underset{\sim}{Q}}$

$${}^c\dot{\underset{\sim}{Q}}\,{}^c\underset{\sim}{Q}^T = \underset{\sim}{W} = \} \quad \underset{\sim}{L} \quad \{ \quad \text{and} \quad {}^c\underset{\sim}{Q}(t_0) = \underset{\sim}{I} \tag{13}$$

where the inverted brackets denote the skew-symmetric part of the expression and $\underset{\sim}{L}$ the velocity gradient. The decomposition into elastic and viscoplastic strain rates in the corotational space frame is additive:

$${}^c\underset{\sim}{D} = {}^c\,\underset{\sim}{Q}^T \{\underset{\sim}{L}\}\,{}^c\underset{\sim}{Q} = {}^c\,\dot{\underset{\sim}{E}}^e + {}^c\,\dot{\underset{\sim}{E}}^p \tag{14}$$

where the brackets denote the symmetric part of the expression.

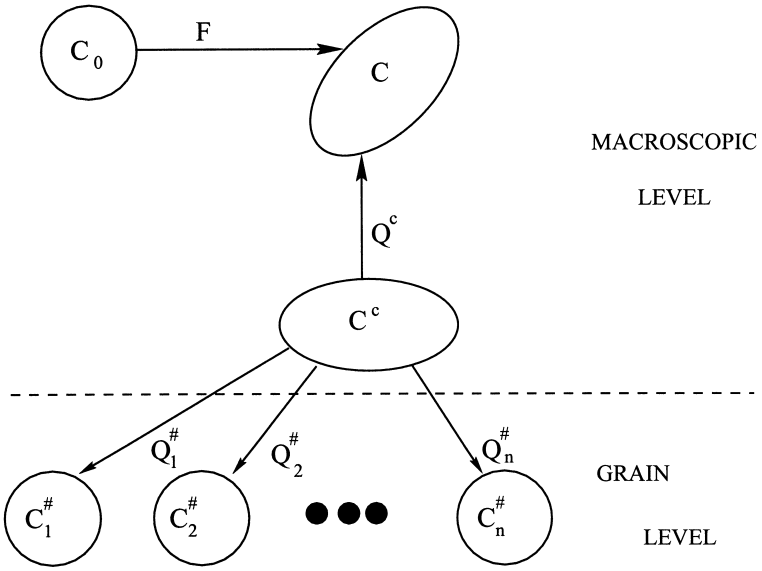

Fig. 1. Configurations representation.

Elasticity is described according to a linear relation:

$$\underset{\sim}{S} = \underset{\sim}{C}^{c}\underset{\sim}{E}^{e} \quad \text{with} \quad \underset{\sim}{S} = \left(\det \underset{\sim}{F}\right) {}^{c}\underset{\sim}{Q}^{T}\underset{\sim}{\Sigma}\,{}^{c}\underset{\sim}{Q} \tag{15}$$

where $\underset{\sim}{\Sigma}$ is the Cauchy stress tensor.

The use of a corotational frame for the expression of the constitutive equations leads to a hypoelastic formulation for the reversible part of the deformation. The drawbacks of the hypoelastic framework are well-known: the final stress state after a closed strain path may differ from the initial one even for a purely hypoelastic solid and the treatment of an anisothermal material responses may lead to difficulties. As a result, an explicit potential like the free energy cannot be given. However, the advantages are the numerical efficiency of this type of model and the simplicity of the extension of classical constitutive equations to a large deformation framework. According to Rougee (1997), the approach involving local objective frames represents a compromise between the weaknesses of hypoelasticity and the arbitrary choice of specific strain measures. An alternative framework for polycrystal plasticity can be found in Mandel (1982). The macroscopic viscoplastic strain rate is given by:

$${}^{c}\dot{\underset{\sim}{E}}^{p} = \sum_{g\in G} f_{g}^{c}\dot{\underset{\sim}{\varepsilon}}^{pg} \tag{16}$$

The local viscoplastic deformation ${}^{c}\dot{\underset{\sim}{\varepsilon}}^{pg}$ proceeds through collective glide of dislocations on activated slip systems:

$${}^{c}\dot{\underset{\sim}{\varepsilon}}^{pg} = \sum_{s} \dot{\gamma}^{s}\{{}^{c}\vec{m}^{sg} \otimes {}^{c}\vec{n}^{sg}\} \tag{17}$$

where ${}^c\vec{m}^{sg}, {}^c\vec{n}^{sg}$ are the slip direction and the normal to the slip plane of phase (g) respectively, defined in the space frame C^c.

The corotational space frame is such as the instantaneous rotation rate in this frame vanishes:

$$ {}^c\underset{\sim}{W} = 0 \tag{18}$$

Taylor-like relations for rotations are assumed:

$$ {}^c\underset{\sim}{\omega}^g = {}^c\underset{\sim}{W} = 0 \tag{19}$$

this allows us to determine the lattice rotation rate:

$$ {}^c\underset{\sim}{\omega}^{eg} = -{}^c\underset{\sim}{\omega}^{pg} \quad \text{with} \quad {}^c\underset{\sim}{\omega}^{pg} = \sum_s \dot{\gamma}^s \{{}^c\vec{m}^{sg} \otimes {}^c\vec{n}^{sg}\} \tag{20}$$

The rotation between ${}^{\#}C^g$ and ${}^cC$ is then given by:

$$ {}^{\#}\dot{\underset{\sim}{Q}}^g \, {}^{\#}\underset{\sim}{Q}^{gT} = {}^c\underset{\sim}{\omega}^{eg} \text{ and } {}^{\#}\underset{\sim}{Q}^g(t_0) = \underset{\sim}{I} \tag{21}$$

The resolved shear stress on slip system (s) in phase (g) is given by:

$$ \tau^{sg} = \underset{\sim}{s}^g : ({}^c\vec{m}^{sg} \otimes {}^c\vec{n}^{sg}) \tag{22}$$

and localisation rule is written in the corotational frame:

$$ \underset{\sim}{s}^g = \underset{\sim}{S} + 2\mu(1-\beta)\left(\underset{\sim}{B} - \underset{\sim}{\beta}^g\right) \quad \text{with} \quad \underset{\sim}{B} = \sum_{g\in G} f_g \underset{\sim}{\beta}^g \tag{23}$$

where the intergranular accommodation variables are given in Eq. (4). It is worth noting that variables **B** and $\underset{\sim}{\beta}^g$ are defined with respect to the corotational frame and thus are invariant with respect to changes of observers.

2.3. Identification procedure

The set of parameters A (material and concentration rule parameters) of the constitutive equations is determined using a classical identification procedure through an automatic software SiDoLo (Pilvin, 1988). This procedure consists on a quantitative comparison $L(A)$ between experimental macroscopic tests Z^{exp}, previously performed on the material, and simulation tests Z^{sim}, using the polycrystalline model β. The role of concentration rule parameters D and δ is to fulfill self-consistency conditions (SCC). These conditions require the comparison of two results:

- resolution of a boundary value problem corresponding to the self-consistent scheme described in Section 2.1.1.
- direct prediction of the polycrystalline model β for the same loading paths (Forest, 1996; Forest and Pilvin, 1995).

The best solution for resolution of the boundary value problem is given by a finite element code where the local stress ($\underset{\sim}{\sigma}^{\mathrm{REF}}$) and strain ($\underset{\sim}{\varepsilon}^{\mathrm{REF}}$) are computed in each phase. The SCC were given by:

$$\underset{\sim}{\sigma}^{\mathrm{REF}} - \underset{\sim}{\sigma}^{\beta} = 0 \quad \text{and} \quad \underset{\sim}{\varepsilon}^{\mathrm{REF}} - \underset{\sim}{\varepsilon}^{\beta} = 0 \tag{24}$$

where $\underset{\sim}{\sigma}^{\beta}$ (resp. $\underset{\sim}{\varepsilon}^{\beta}$) correspond to the stress (resp. strain) in each phase predicted by the polycrystalline model β. The optimization problem is then solved by using a cost function $L_p(A)$ defined by:

$$L_p(A) = L(A) + \Sigma\left|\underset{\sim}{\sigma}^{\mathrm{REF}} - \underset{\sim}{\sigma}^{\beta}(A)\right| + \left|\underset{\sim}{\varepsilon}^{\mathrm{REF}} - \underset{\sim}{\varepsilon}^{\beta}(A)\right| \tag{25}$$

The hereabove identification with EF technique costs, for the studied aggregate, large computation time on a SILICON origin 2000 computer. In order to reduce the computation time, finite element computation are replaced by Berveiller–Zaoui polycrystalline model computation using the concentration rule (2). Local stresses (local strains) computations with polycrystalline β model and polycrystalline Berveiller–Zaoui model are performed for monotonous loading (uniaxial test) by using isotropic orientation distribution function made of 240 equivalent orientations. The different steps of the procedures are summarized in Fig. 2.

At room temperature, steel viscosity is weak and the elastoviscoplastic framework of the polycrystalline model β is assumed close to the elastoplastic framework of the

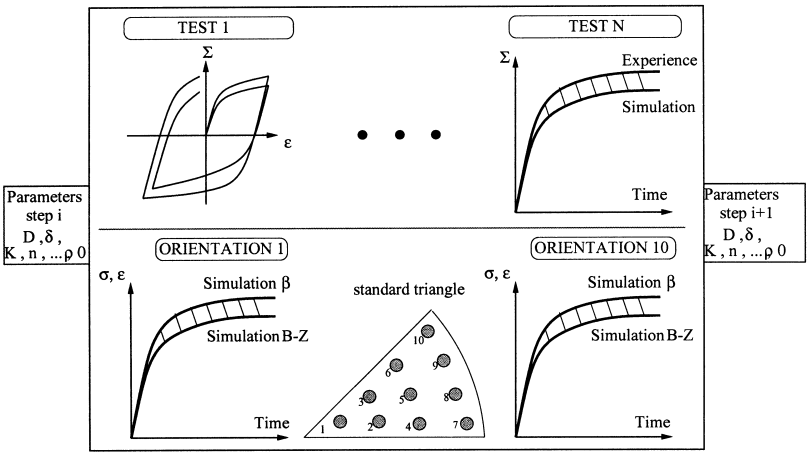

Fig. 2. Identification procedure.

polycrystalline model Berveiller–Zaoui. Nevertheless, in order to check the validity of this hypothesis, the local stress and strain fields computations obtained by the polycrystalline Berveiller–Zaoui model are compared to finite element results, for two specific orientations of the inclusion (phase a: $\langle 001\rangle // \overrightarrow{e_z}$ and phase b: $\langle 111\rangle // \overrightarrow{e_z}$). Finite element computation are performed with Abaqus code, using 8 nodes quadratic axisymetric elements. The two inclusions are embedded in "infinite" HEM matrix with homogeneous strain prescribed at the boundary (Fig. 3c). In each case, the matrix is defined by the polycrystalline model with Berveiller–Zaoui transition rule. The ratio between the inclusion and matrix dimension is taken equal to 5.

The local stress-elongation curves are plotted on Fig. 3a and b. A good agreement is obtained between the two computations, pointing out large intergranular heterogeneities of the aggregate. Intragranular heterogeneities are also observed in inclusion of Fig. 3c but they are weak and then consistent with the homogeneous stress field predicted by the Berveiller–Zaoui polycrystalline model.

3. Results

3.1. Experimental material and procedure

The material used in this study is an interstitial free steel, with an average grain size of 20 μm, cold rolled then annealed. It is thinned down to a final thickness of 0.9 mm. To characterize the amplitude of the strain path changes, we use a scalar parameter θ introduced by Schmitt et al. (1994):

$$\theta = \frac{\dot{E}_1 : \dot{E}_2}{\left|\dot{E}_1\right|\left|\dot{E}_2\right|} \tag{26}$$

In this formula, $\dot{E}_1$ and $\dot{E}_2$ represent the prestrain and strain rate tensors respectively, $\left|\dot{E}_1\right| = \sqrt{\dot{E}_1 : \dot{E}_1}$ and the symbol (:) corresponds to the double-contracted tensor product. According to (26) a monotonic test corresponds to 1, a Bauschinger test to -1 and a deformation sequence is called orthogonal when $\theta = 0$. All tests performed in this paper are given in Table 1.

Table 1
Tests performed in the present investigation

θ	Sequence	Test	Denomination	Temperature
1	Monotonic	Uniaxial tension	UT90	Room
1	Monotonic	Uniaxial tension	UT90T	353 K
1	Monotonic	Plane tension	TP	Room
−1	Bauschinger	Cyclic planar shear	CIS	Room
−0.15	Quasi orthogonal	TP + uniaxial tension at 90°	TP90	353 K
0.8	Quasi monotonic	TP + uniaxial tension at 0°	TP0	353 K

3.1.1. Monotonic loading

For uniaxial tension tests, samples had a 8 mm gage length and 3 mm gage width. The applied rate of the macroscopic displacement was 0.8 μm s^{-1},and corresponded to a macroscopic strain rate of about 10^{-4} s^{-1}. Tensile tests were performed at two temperatures, 293 and 353 K, in the transversal direction.

For plane tension test, large samples (200×50 mm^2) were used and strained in the rolling direction. The rate of macroscopic strain rate was about 10^{-3} s^{-1}. Grids were laid on the samples in order to verify plane strain conditions, i.e. $|\varepsilon_2| < \frac{1}{10}\varepsilon_1$. Effective strain ε_1 was deduced from thickness measurements by SOLLAC.

3.1.2. Strain path changes

In the present investigation, cyclic planar simple shear tests were performed ($\theta = -1$). In this test, the rectangular ($50\times3\times0.9$ mm^3) specimens were fixed by two sets of grips submitted to a parallel displacement (G'sell et al., 1983). Macroscopic shear strain rate was close to 10^{-4} s^{-1} and the shear direction was perpendicular to the rolling direction.

In order to obtain a quasi orthogonal strain path, uniaxial tension samples were cut out in the homogeneous area of plane tension samples, at 90° of prestrain direction (Fig. 4). In this sequence of loading path, θ was close to -0.15, due to anisotropic

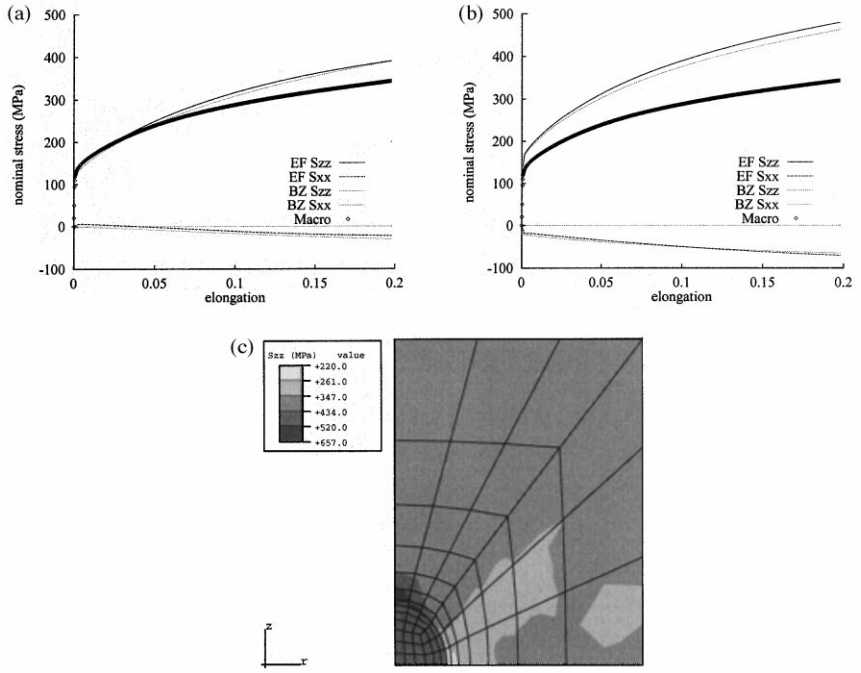

Fig. 3. Comparison between FE and polycrystalline model Berveiller–Zaoui. (a) Phase a: (001) oreintation for inclusion; (b) phase b: orientation for inclusion; (c) finite calculation of inclusion embedded in polycrystal matrix. S_{zz} stress for phase b (elongation = 0.2).

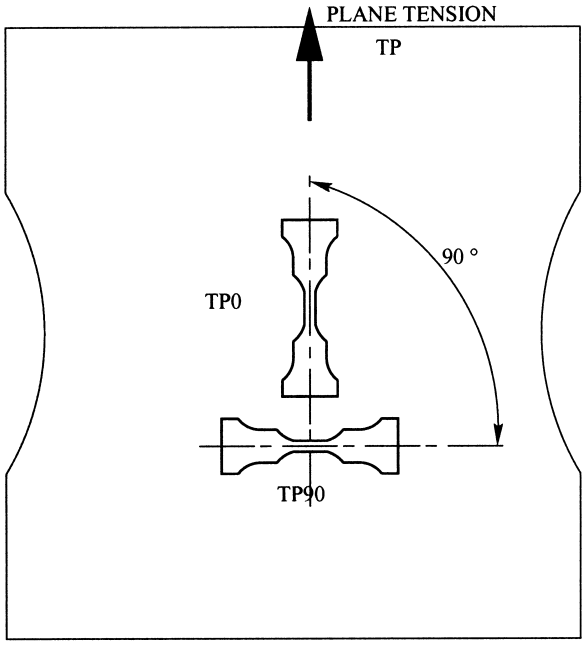

Fig. 4. Sample preparation.

behavior (Lankford coefficient was close to two). For comparison, some samples were cut out in the same direction of prestrain ($\theta \simeq 0.8$). In the two cases, uniaxial tension tests were performed for an equivalent prestrain of 18%. It is worth noting that plastic instability occurred during the second path for small strains. In this paper, only the stress-strain curves before instabilities (Hoc, 1999) are reported and analyzed.

3.2. Hardening matrix

For B.C.C. polycrystals, the predominant deformation mechanism are crystallographic glides on the twelve systems $\{110\}\langle 111\rangle$ and on the twelve systems $\{112\}\langle 111\rangle$. The polycrystalline model computation have been performed with an orientation distribution function, taken under a discrete form corresponding to 891 orientations and, in the hereafter computation, the 24 crystallographic glides systems have been taken into account. It is worth noting that with only the first twelve systems, the obtained results of the simulation do not agree with experiments.

For the sake of simplicity, we first introduce in our computation a simplified hardening matrix composed of two terms, namely the self hardening (a^{ss}) and the latent hardening (a^{ls} with $s \neq l$) coefficients. For monotonous deformation, a good agreement has been obtained between the experimental results and the numerical curves (Fig. 5a). However, for the change of strain path (plane tension-uniaxial tension), the simplified hardening matrix leads to a large discrepancy between experimental and numerical results (Fig. 5b).

To solve this problem, a 24×24 hardening matrix composed of six different terms has been considered. The interactions between slip systems have been classified in different types as they belong to the same system, to colinear system or to no colinear system. Moreover, interaction between planes {110} have been assumed smaller than interactions between planes {112}. Table 2 gives all interaction coefficients.

The simulations have been performed with $k_1 = 1$, $k_2 = 1.15$, $k_{p1} = 1.05$, $k_{p2} = 1.05$, and $k_{s0} = 1.3$. A good agreement has been obtained between numerical results and experimental curves for plane tension-uniaxial tension and cyclic shear tests as shown in Fig. 6b and a, respectively. It is worth noting that only isotropic hardening is taken into account. In order to obtain bests results on elasto-plastic transition during cyclic shear test, intragranular kinematics hardening could be introduced.

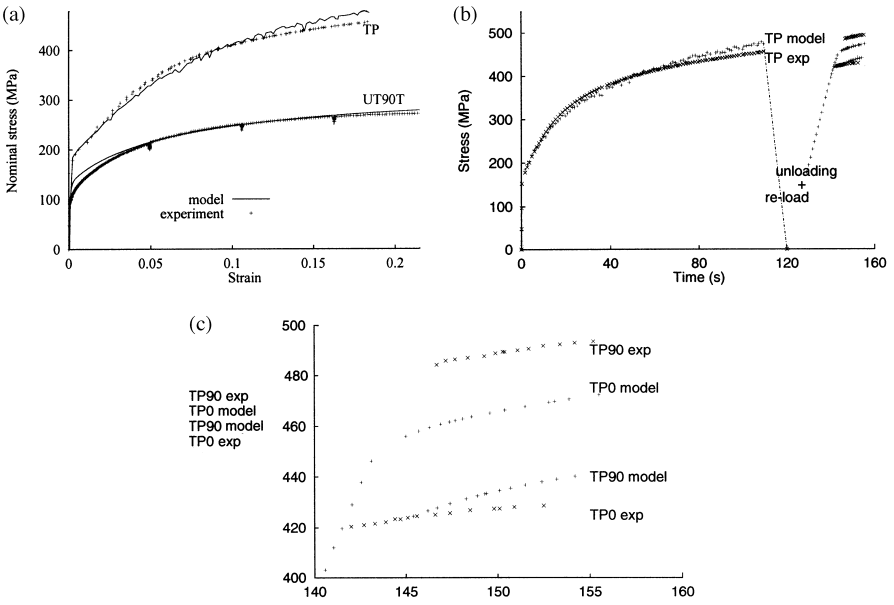

Fig. 5. Matrix interaction with two coefficients. (a) monotonous loading; (b) sequential loading path. Stresses at reloading do not agree. (c) Zoom.

Table 2
Matrix interaction coefficients

Plane	{110}∩{110}	{110}∩{112}	{112}∩{112}
Same	a_0		$k_{s0}a_0$
Colinear	k_1a_0	$k_{p1}a_0$	$k_{s0}k_1a_0$
No colinear	$k_2k_1a_0$	$k_{p2}k_{p1}a_0$	$k_{s0}k_2k_1a_0$

3.3. Texture evolution

The previous identifications have been carried out on the macroscopic stress–strain curves, but other properties more local can be predicted like the texture evolution, which is often one of the main objectives of polycrystal modelling at large strains (Bacroix and Hu, 1995). Poles figures {200}, {220} and {211} have been measured by X-ray diffraction techniques before and after each test in a reference frame, linked to rolling direction. The orientation distribution function (ODF) has been computed using vector method (Ruer and Buro, 1977) where the texture is described as a finite sets of weighted orientations.

The pole figures corresponding to the initial texture are given in Fig. 7a and b for two representation modes (equal intensity levels and points). These pole figures are characteristic of a typical steel texture (Ceccaldi et al., 1994), i.e. mostly composed of a {111} ⟨uvw⟩ fibre, called α-fiber.

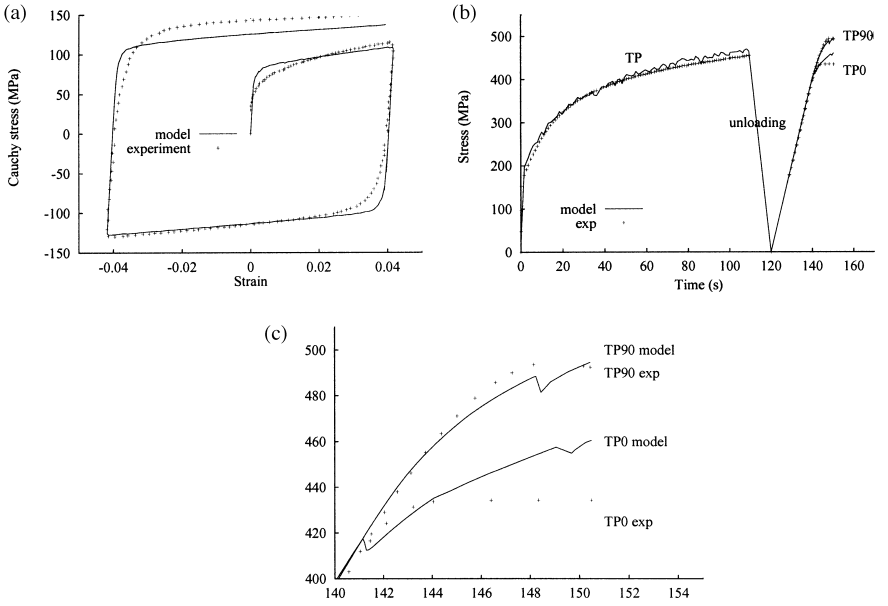

Fig. 6. Matrix interaction with six coefficients. (a) Cyclic plane shear test; (b) sequential loading path; (c) zoom.

Table 3
Materials parameter

T (°C)	E (GPa)	ν	a_0	K	τ_0 (MPa)	G_c (nm)	n	$\dot{\gamma}_0$ (s^{-1})	ρ_0 (m^{-2})
20					30	5			
	200	0.3	0.4	20			15	1.14	64.10^9
80					20	10			

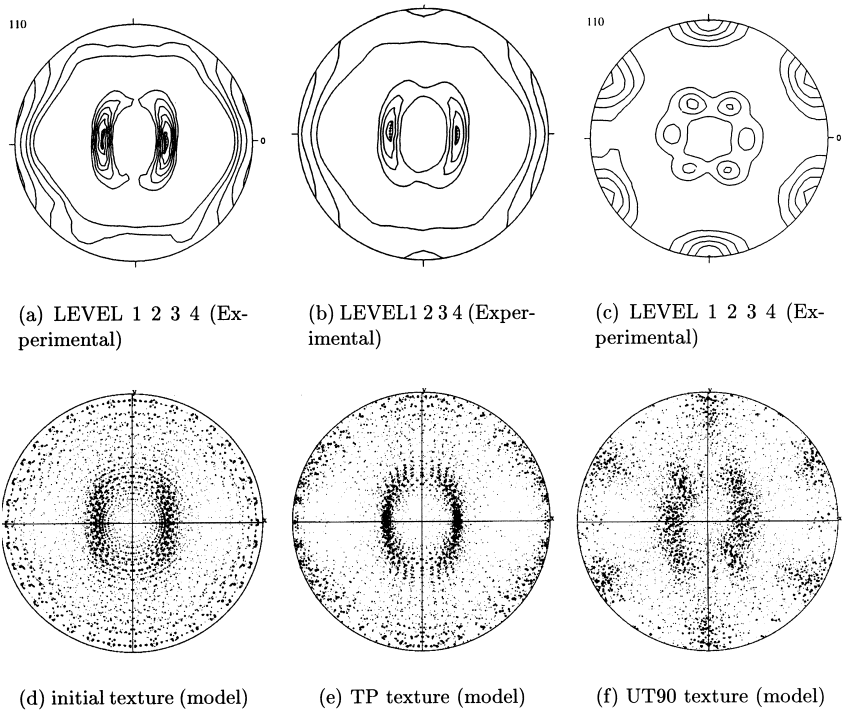

(a) LEVEL 1 2 3 4 (Experimental)

(b) LEVEL1 2 3 4 (Experimental)

(c) LEVEL 1 2 3 4 (Experimental)

(d) initial texture (model)

(e) TP texture (model)

(f) UT90 texture (model)

Fig. 7. Comparison between polycrystal model and experimental results. Poles figures 110.

Good agreements have been also obtained between numerical and experimental textures corresponding to the plane tension tests and to the uniaxial tension test along the transversal direction. In the first case, a classical reinforcement of α-fiber has been obtained, whereas in the second case, the final texture correspond to a 30° rotation around the normal direction of the sheets steel.

Let us note that the form of the hardening matrix has a weak influence on texture.

3.4. Discussion

3.4.1. Concentration rule parameters and remaining material parameters

The tuning parameters of the concentration rule and the materials parameters have been identified. The values of the two concentration rule parameters D (resp. δ) are close to 700 (resp. 0.02). These parameters allow to determine the evolution of the $\underset{\sim}{\beta}$ variable:

$$\dot{\underset{\sim}{\beta}}^g = \dot{\underset{\sim}{\varepsilon}}^{pg} - 700\left(\underset{\sim}{\beta}^g - 0.02\underset{\sim}{\varepsilon}^{pg}\right)\left\|\dot{\underset{\sim}{\varepsilon}}^{pg}\right\| \tag{27}$$

The aim of this variable is to introduce intergranular heterogeneities observed during experimental tests and to simulate complex loadings. Fig. 8a shows locals

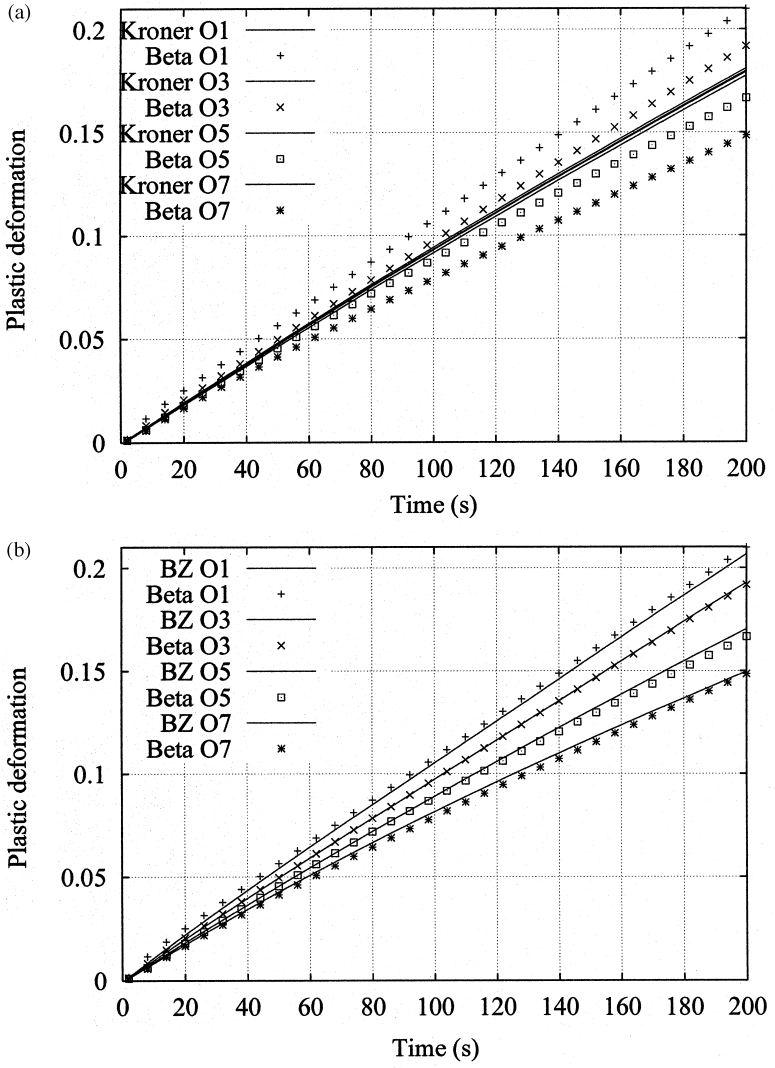

Fig. 8. Local deformation for 4 phases. (a) Comparison between Kröner and β model; (b) comparison between BZ and β model.

deformations of four phases (O1, O3, O5, O7) which orientations are given in Fig. 2 for Kröner and β polycrystalline model. These curves are obtained during an uniaxial test with initial isotropic texture.

The results show a very homogeneous behavior of different phases by using Kröner model. By contrast, β polycrystalline modelgives heterogeneous behavior ($\sim$20%) which corresponds to experimental observation. Moreover β and Berveiller–Zaoui models are quite similar (see Fig. 8b) for monotonous loading.

Concerning the other parameters given in Table 3, our results point out that τ_0 (lattice friction) and G_c (parameter associated with the annihilation process of dislocation dipoles) depend on the temperature. Their evolution with temperature fits with E. Rauch's results (Rauch and Thuillier, 1993) obtained for simple shear tests on mild steel. The computed initial main free path

$$L_s = \frac{K}{\sqrt{23\rho_0}} = 16.2\,\mu\text{m}$$

is close to grain size. It is worth noting that the present investigation, which is based on a phenomenological model taking into account a physical description of the plasticity mechanisms and on an anisotropic work-hardening, leads to physical values of all material parameters (Rauch, 1993).

3.4.2. Study of yield stress

The simulation of the second loading path agrees with the experiments. Let us now examine the physical mechanisms leading to two different "conventional" ($\varepsilon_p = 0.2\%$) yield stresses after reloading. The "conventional" yield stresses σ_a^0 and σ_a^{90} are defined in Fig. 9 and correspond to the monotonic and orthogonal paths respectively. Our experimental results point out that σ_a^{90} is higher than σ_a^0. Such results agree with Raphanel et al. (1987). According to these authors, the yield stress after reloading is the highest, the closest to zero is θ.

The difference between the two conventional yield stresses can be explained by the macroscopic evolution of the anisotropy of the polycrystal during the first load or (and) by the anisotropy of the hardening matrix. Concerning the global anisotropy, we have computed the yield surface for the initial material and after a 18% prestrain in plane tension. The two surfaces are given in Fig. 10. They are obtained by computing different strain paths (0–360° with respect to rolling direction by step of 10°). The equivalent plastic strain offset used to define the numerical yield stress has been

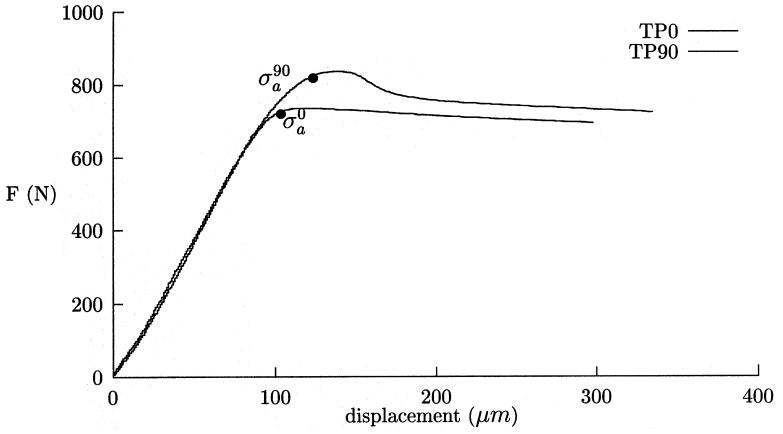

Fig. 9. Experimental test TP0 and TP90.

taken equal to 0.01%. The weak value of offset allows us to define the beginning of microplasticity stage.

According to our computation, the numerical yield stress in the rolling direction σ_e^0 is slightly greater than σ_e^{90} in the orthogonal direction, but the computed values can not explain the experimental results. By contrast, with an offset of 0.2% corresponding to the conventional yield stresses, numerical results fit to experimental results: $\sigma_a^0 = 493\,\text{MPa}$ and $\sigma_a^{90} = 542\,\text{MPa}$.

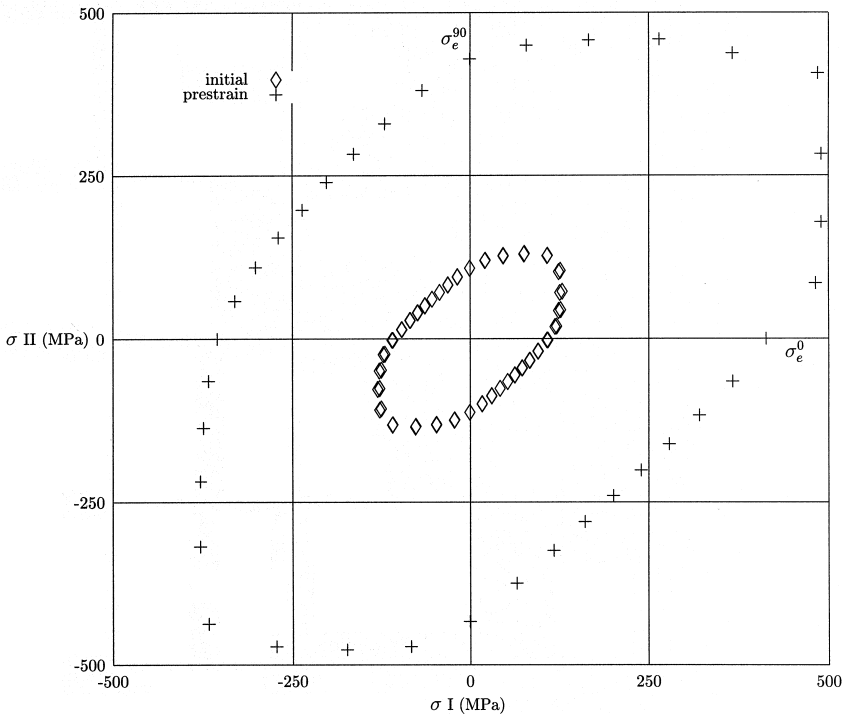

Fig. 10. Yield surfaces.

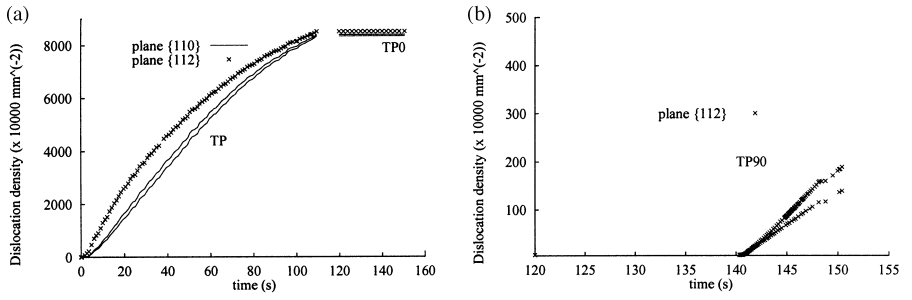

Fig. 11. Dislocation evolution for loading path change. (a) Prestrain and second loading at 0°; (b) new active slip system during second loading at 90°.

According to our experimental results, the conventional yield stresses are dependent on the microplasticity stage. In the case of the orthogonal path, the transition between linear elastic and microplasticity stages is smooth and the stress-strain curve is parabolic. In the quasi monotonic stage, a sharp transition followed by a plateau is observed ($\sigma_a^0 = \sigma_e^0$). The conventional yield stress σ_a^{90} amplitude can be related to the anisotropy of the identified hardening law which takes into account the different evolutions of the densities of dislocations on the different slip systems. As a matter of fact, it must be noticed that during the quasi monotonic strain path, no significant increases of dislocation densities take place. On the contrary, for quasi orthogonal strain path, new slip systems which were latent during the prestrain become active (Fig. 11).

These results point out that the microplasticity stages strongly depend on the "anisotropy" of the densities of dislocations built during the first loading.

4. Conclusion

The mechanical behavior of IF-Ti low carbon steel was studied under various loading conditions. Viscoplatic behavior and hardening laws based on a physical description of crystalline plasticity were first postulated. The identification of the physical parameters were performed thanks to a pragmatic polycrystalline approach. Whereas the classical fully self-consistent scheme leads to an intricate integral equation which must be solved at each step, the proposed approach is based on an explicit formulation of the concentration rule, involving additional variable characteristics of each phase. Such an approach, shortens the computation time and gives numerical results in good agreement with experimental data such as stress–strain curves and crystalline texture. A particular attention has been paid to physical parameters of the hardening law. The comparisons between simulations and experiments point out the necessity of an accurate description of the mechanisms of microplasticity. The most important results of the identification can be summarized as follow.

1. Twenty four slip systems $\{110\}\langle 111\rangle$ and $\{112\}\langle 111\rangle$ must be introduced to describe the experimental tests. This result fits with Jaoul's theory of pencil glide.
2. The hardening matrix is composed of 6 different terms bound to different interactions between slip systems $\{110\}$, $\{112\}$. The classical description of the hardening matrix composed of two terms corresponding to the self hardening and the latent hardening does not hold here.
3. An accurate description of the behavior of polycrystals after a prestrain needs an accurate description of the evolutions of densities of dislocation on each slip systems. The different evolutions of dislocations densities on each slip systems, [see Eq. (9)] allow to explain reloading stress level after a prestrain in plane tension. As a matter of fact, anisotropic hardening depends on the activated slip systems and increases with the amplitude of the prestrain. The stress level after reloading is bound to the density of obstacles on latent slip systems previously activated.

The results of the simulation based on this simplified polycrystalline approach fit with experimental observations, providing an accurate description of the mechanisms of plasticity and of hardening matrix.

Acknowledgements

The authors are grateful to Dr. Ph. Pilvin and to Professor C. Rey for stimulating discussions. The authors would like to thank T. Chauveau (LPMTM, Université Paris 13, Villetaneuse, France) for providing experimental texture.

References

Bacroix, B., Hu, Z., 1995. Texture evolution induced by strain path changes in low carbon steel sheets. Metall. Mater. 26, 601–613.

Berveiller, M., Zaoui, A., 1979. An extension of the self-consistent scheme to plastically flowing polycrystals. J. Mech. Phys. Solids 26, 325–344.

Berveiller, M., Zaoui, A., 1998. Modèle de passage du monocristal au polycristal en plasticité. In: Ecole thématique du CNRS, Août.

Cailletaud, G., 1991. A micromechanical approach to inelastic behavior of metals. Int. J. Plasticity 8 (1), 55–74.

Ceccaldi, C., Yala, F., Baudin, T., Penelle, R., Royer, F., Arminjon, M., 1994. Deformation textures and plastic anisotropy of steels using the Taylor and non homogeous models. Int. J. Plasticity, 10 (6).

Essman, U., Mughrabi, H., 1979. Annihilation of dislocations during tensile and cyclic deformations and limits of dislocation densities. Phil. Mag. A40, 731–756.

Forest, S., 1996. Mechanical Modeling of Non-homogeneous Deformation of Single Crystals. PhD thesis, Ecole des Mines de Paris and Communitatis Europae.

Forest, S., Pilvin, P., 1995. Modelling the cyclic behaviour of two phase single crystal nickel-base superalloys. In: Proceedings of the IUTAM Symposium on Micromechanisms of Multiphase Materials. Kluwer, Sèvres, pp. 51–58.

Forest, S., Pilvin, P., 1999. Modelling finite deformation of polycrystals using local objectives frames. ZAMM Z. Angew. Math. Mech. 79, S199–S202.

Franciosi, P., 1984. Etude Théorique et Expérimentale du Comportement Elastoplastique des Monocristaux Métalliques se Déformant par Glissement: Modélisation pour un Chargement Complexe Quasi Statique. PhD thesis, Université Paris XIII, avril 1984.

Franciosi, P., 1985. The concept of latent hardening and strain hardening in metallic single crystals. Acta Metal. 33, 1601–1612.

Ghosh, A.K., Backofen, W.A., 1973. Strain hardening and instability in biaxiality stretched sheets. Metall. Trans. 1973.

G'sell, C., Boni, S., Shrivastava, S., 1983. Application of plane simple shear test for determination of the plastic behaviour of solid polymers at large strain. J. Mater. Sci. 18, 903.

Hill, R., 1965. Continuum micro-mechanisms of elastoplastic polycrystals. J. Mech. Phys. Solids 13, 89–101.

Hiwatashi, S., Van Bael, A., Van Houtte, P., Teodosiu, C., 1998. Prediction of forming limit strains under strain path changes: application of an anisotropic model based on texture and dislocation structure. Int. J. Plasticity 14 (7), 647–669.

Hoc, T., 1999. Etudes Experimentale et Numerique de la Localisation de la Deformation Lors de Changement de Trajet Dans Un Acier Doux. PhD thesis, Ecole Centrale Paris.

Hu, Z., Rauch, E.F., Teodosiu, C., 1992. Work-hardening behavior of mild steel under stress reversal at large strains. Int. J. Plasticity 8, 839–856.

Korbel, A., Martin, P., 1988. Microstructural events of macroscopic strain localization in prestrained tensile specimen. Acta Metal. 36 (9), 2575–2586.

Kroner, E., 1961. Zur plastischen verformung des vielkristalls. Acta Metal. 9, 155–161.

Ladeveze, P., 1980. Sur la Théorie de la Plasticité en Grandes Déformations. Technical report, ENS Cachan, Novembre 1980.

Mandel, J., 1982. Définition d'un repère privilégié pour l'étude des transformations anélastique du polycrystal. Journal de mécanique théorique et appliquée 1, 7–23.

Pilvin, P., Identification des paramètres de modèles de comportement. In: Oytana et al. (Eds.), International Seminar on Mécamat "the Inelastic Behaviour of Solids". Besancon, pp. 155, 1988.

Pilvin, P., 1994. The contribution of micromechanical approaches to the modelling of inelastic behaviour of polycrystals. In: Société Francaise de Métallurgie et de matériaux, vol. I, p. 31–45, May 1994.

Raphanel, J.L., Rauch, E.F., Shen, E.L., Schmitt, J.-H., 1987. Shear of prestrained steel specimen. Scripta Metal 21, 1087–1090.

Rauch, E.F., 1993. Etude de l'Ecrouissage des Métaux. PhD thesis, I.N.P. Grenoble.

Rauch, E.F., G'sell, C., 1989. Flow localization induced by a change in strain path in mild steel. Materials Science and Engineering A111, 71–80.

Rauch, E.F., Thuillier, S., 1993. Plasticity and unstable flow of mild steel. Archives of Metallurgy 38, 167–177.

Rougee, P., 1997. Mecanique des grandes transformations: mathematiques at applications. In: Springer 1997.

Ruer, D., Baro, R., 1977. Méthode vectorielle d'analyse de la texture des matériaux polycrystallins de réseau cubique. J. Appl. Cryst. 10, 458.

Schmitt, J.H., Shen, E.L., Raphanel, J.L., 1994. A parameter for measuring the magnitude of a change of strain path: validation and comparison with experiments on low steel. Int. J. Plasticity 10 (5), 535–551.

Teodosiu, C., Sidoroff, F., 1976. A theory of finite elastoviscoplasticity of single crystals. Int. J. Engng Sci. 14, 165–176.